IN-27
121337

P-24
476956

Analysis of Precracking Parameters and Fracture Toughness for Ceramic Single-Edge-Precracked-Beam Specimens

Sung R. Choi and Abhisak Chulya
Cleveland State University
Cleveland, Ohio

and

Jonathan A. Salem
Lewis Research Center
Cleveland, Ohio

NASA

ANALYSIS OF PRECRACKING PARAMETERS AND FRACTURE TOUGHNESS

FOR CERAMIC SINGLE-EDGE-PRECRACKED-BEAM SPECIMENS

Sung R. Choi* and Abhisak Chulya*
Cleveland State University
Cleveland, Ohio 44115

Jonathan A. Salem
National Aeronautics and Space Administration
Lewis Research Center
Cleveland, Ohio 44135

SUMMARY

The single-edge-precracked-beam (SEPB) method involves creation of a straight-through crack from an indentation crack. The straight-through crack is developed by applying a controlled bending load to a specimen via a precracking fixture. The fixture induces a sequence of (1) stable growth of the initial indentation crack, (2) pop-in, and then (3) arrest—thereby forming a straight-through precrack. The effects of indentation load on precracking load as well as on precrack size were studied for experimental variables such as specimen width, fixture span, and material. Finite element analysis was used to obtain the stress distribution and stress intensity factor, thus providing a quantitative prediction of the precracking load and precrack size for silicon nitride, alumina, silicon carbide, and two silicon carbide whisker-reinforced silicon nitrides. Fracture toughness values obtained from the SEPB method were compared with those obtained from other methods.

INTRODUCTION

The single-edge-precracked-beam (SEPB) method, first applied to ceramics by Nose and Fujii (ref. 1), produces a sharp straight-through precrack in a ceramic beam specimen so that the specimen can be evaluated for fracture toughness. In the SEPB method, originally termed the "bridge"-indentation method (ref. 2), a straight-through crack is developed from a Vickers indentation flaw placed in the center of the tensile surface of a specimen. The crack develops when a controlled bending load is applied via a precracking fixture. The fixture induces a sequence of (1) stable crack growth of the initial indent crack, (2) pop-in, and then (3) arrest—thereby producing a sharp straight-through precrack.

The effects of precracking parameters such as indentation load, precracking load, and precrack size have been studied experimentally and analytically by Warren and Johanneson (ref. 2) and Bar-On et al. (ref. 3). However, their studies did not include in-depth analyses of these parameters on the basis of "indentation" and conventional fracture mechanics principles.

In this report, the effects of indentation load on precracking load as well as on precrack size are presented as a function of fixture and specimen configurations. Strain gaging, finite element analysis, and indentation strength data were incorporated to obtain the stress distribution and stress intensity factor, thereby obtaining analytical solutions of the precracking parameters as a function of indentation load. The analytical solutions were compared with the experimental results obtained for silicon nitride, alumina, silicon carbide, and two SiC whisker-reinforced silicon nitrides. Fracture toughness was also determined from the precracked specimens of the tested materials and compared with the values obtained from other methods.

*NASA Resident Research Associates at Lewis Research Center, Cleveland, OH.
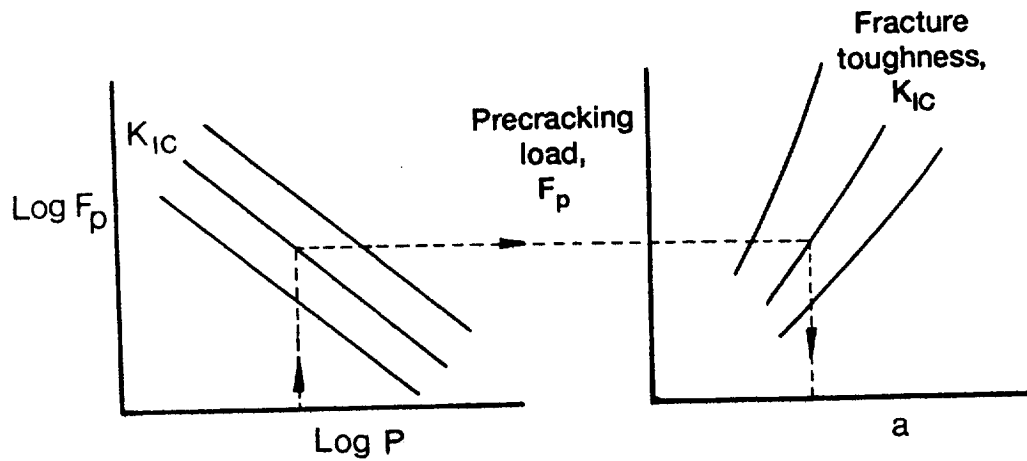
Figure 17.—Schematic to illustrate a prediction of a required indentation load, P, for a given precrack size, a, (and vice versa).
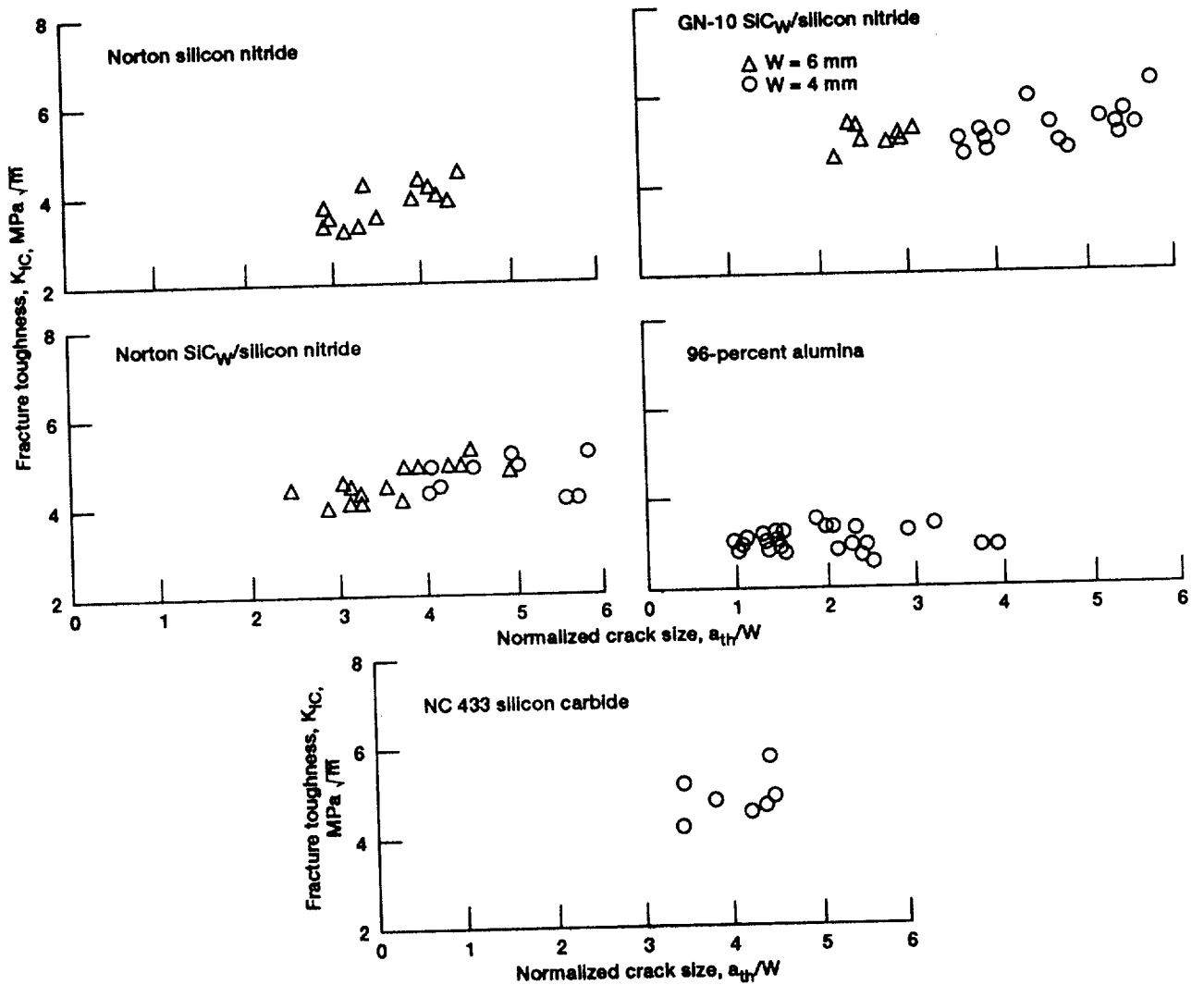

Figure 18.—Summary of fracture toughness as a function of crack size by SEPB method for five test materials.

Finally, strain gages were used with some of the specimen and fixture configurations to estimate the tensile stress as a function of applied compressive load for comparison with finite element analysis and indentation strength results.

ANALYSES

Indentation Fracture

For indentation cracks produced in ceramics and glasses by a Vickers indenter and subjected to an applied remote stress, the net stress intensity factor K, assuming a half-penny crack configuration, consists of two terms (ref. 6):

$$K = K_r + K_a$$
$$= \frac{\Sigma_r P}{a^{3/2}} + \Omega \sigma_a \sqrt{a} \tag{1}$$

The first term, K_r, is the mode I residual stress intensity factor due to residual stresses produced by the elastic/plastic mismatches of indentation. The residual stress is represented by a point force acting on the center of the half-penny crack plane. The second term, K_a, is the mode I applied stress intensity factor due to an applied remote stress σ_a. Σ_r is a material/indenter geometry constant associated with the residual contact stress, P is the indentation load, a is the crack size, and Ω is the crack geometry factor. The functional dependency of K on a indicates that stable crack growth with conditions of $K \geq K_{IC}$ and $dK/da < 0$ proceeds during loading until an instability point where $dK/da = 0$ and $K = K_{IC}$ are fulfilled. Using this instability condition, one can obtain from equation (1) (ref. 6)

$$\sigma_f = \frac{3K_{IC}}{4\Omega\sqrt{a_f}} \tag{2a}$$

$$a_f = \left[\frac{4\Sigma_r P}{K_{IC}}\right]^{2/3} \tag{2b}$$

where σ_f and a_f are, respectively, the fracture strength and the critical crack size at instability. The stable crack growth occurs from the as-indented initial crack size a_i to the end of stable crack growth at size a_f. Also, from equation (2), the fracture strength as a function of indentation load is determined to be

$$\sigma_f = \left[\frac{3K_{IC}^{4/3}}{4^{4/3}\Omega\Sigma_r^{1/3}}\right]P^{-1/3} \tag{3}$$

When the indented specimen is gradually loaded in the precracking fixture, the relationship between the compressive load F_a and the maximum applied tensile stress σ_a induced in the specimen is elastic. Hence,

3

$$\sigma_a = \alpha F_a \tag{4}$$

where

$$\alpha = f(S,L,W,t,E,\nu)$$

where α is a proportionality constant that depends on the inner span S and outer span L of the fixture, and on the width W, thickness t, Young's modulus E, and Poisson ratio ν of the specimen. With increasing applied load, the indent crack is subjected to continuous stable crack growth until the instability point (σ_f and a_f) where the half-penny-shaped indent crack pops-in to form a straight-through crack. Therefore, precracking occurs at the instability condition of the indent crack when

$$F_a = F_p \quad \text{with} \quad \sigma_a = \sigma_f \tag{5}$$

where F_p is defined as the precracking load.

Now by using equations (3) to (5), the precracking load F_p can be determined from

$$F_p = \frac{1}{\alpha}\sigma_f \tag{6a}$$

$$F_p = \frac{1}{\alpha(S,L,W,t,E,\nu)}\left[\frac{3K_{IC}^{4/3}}{4^{4/3}\Omega\Sigma_r^{1/3}}\right]P^{-1/3} \tag{6b}$$

The residual contact stress constant Σ_r is an empirical expression given by reference 7

$$\Sigma_r = \phi\left(\frac{E}{H}\right)^{1/2} \tag{7}$$

where H is the material hardness and ϕ is a calibration constant ($\phi \approx 0.016$ for the Vickers indenter). Substituting equation (7) into equation (6) yields

$$F_p = \frac{1}{\alpha(S,L,W,t,E,\nu)}\left[\frac{\Phi K_{IC}^{4/3}H^{1/6}}{\Omega E^{1/6}}\right]P^{-1/3} \tag{8}$$

where $\Phi = 3/(4^{4/3}\phi^{1/3})$. This equation shows that, for a given indentation load and a given fixture configuration, the precracking load is a strong function of fracture toughness, but a weak function of hardness-to-Young's modulus ratio (H/E). Also, note that E and H do not differ significantly in advanced ceramic materials. For a given material and fixture, a plot of log F_p versus log P should yield a slope of $-1/3$, according to equation (8).

The proportionality constant α can be evaluated by strain gaging specimens, finite element analysis of the system, or by the indentation strength method. In the indentation strength method, indentation strengths are determined as a function of indentation load, and then these indentation-strength/indentation-load data are

4

combined with the precracking-load/indentation-load data, thereby yielding the constant α, according to equations (3) and (6).

Finite Element Analysis

Finite element analysis was used to evaluate the proportionality constant α as a function of S, W, and E. The analysis also was used to estimate precrack sizes. The mesh used in this study is presented in figure 2. The following assumptions were made regarding boundary conditions:

(1) There is a two-dimensional plane strain condition.

(2) The upper fixture made of silicon nitride is rigid and provides a uniform compressive load along the upper surface of the specimen.

(3) The lower fixture made of hardened tool steel is not rigid, but deformable.

(4) No friction exists at the contact surfaces between the specimen and the upper fixture.

(5) The specimen and the lower fixture are perfectly bonded.

The third and fifth assumptions were found to be very important and realistic because a rigid body assumption initially made for the lower fixture resulted in an erroneous stress distribution. The fixed values of $L = 18$ mm and $t = 3$ mm were used throughout the analysis.

Typical stress contours are shown in figure 3, where σ_{xx} is plotted for $S = 4$ mm and $W = 4$ mm for the material. This result shows that the stress distribution through the beam width is not symmetric with respect to the central axis of the specimen. The neutral axis is shifted toward the x axis. Although not presented here, the shear stress σ_{xy} along the y axis was found to be negligibly small in comparison to σ_{xx}.

A summary of the evaluated α as a function of S and W is presented in figure 4. Here, α was obtained from equation (4) by evaluating $\sigma_{xx}(\text{max})$ as a function of F_a in megapascals per kilonewtons. This figure shows that α increases with decreasing W and increasing S. Note that the simple beam theory is approximately applicable to the σ_{xx}-S relation, but inapplicable to the σ_{xx}-W relation (note that in the simple beam theory: $\sigma_{xx} \propto S/W^2$) for the SEPB specimen loaded via the precracker fixture. The effect of E on α in a range of $E = 290$ to 330 GPa was found to be insignificant.

Figure 5 shows the stress intensity factor as a function of the straight-through crack size for different levels of precracking load ($S = W = 6$ mm). The stress intensity factors were obtained by varying the crack size for each level of precracking load. Here, the influence of residual contact stress due to indentation (i.e., K_r field) was neglected, since precrack size is, in general, more than 10 times the indentation crack size. The quasi-static stress intensity factor was utilized to predict a precrack size for a given precracking load. Note that the difference between K_{IC} and K_{Ia} for dynamic crack arrest was assumed to be negligibly small. Figure 6, reconstructed from the results of figure 5, summarizes F_p as a function of precrack size for different levels of fracture toughness. These results indicate that precrack size increases with decreasing K_{IC} for a given precracking load. However, unlike the F_p - P relation (eq. (8)), there is no closed-form solution relating the precrack size and F_p.

5

Sequence of Precracking

The sequence of crack pop-in to form the straight-through crack (which now can be illustrated according to equation (1) and the finite element analysis (fig. 5)) is depicted in figure 7. The net stress intensity factor K is plotted as a function of crack size a for different levels of the applied stress. As the applied compressive load increases, K of an indentation crack increases, resulting in stable crack growth, Δa_i, with conditions of $K \geq K_{IC}$ and $dK/da < 0$ at $a = a_i + \Delta a_i$. With a further increase in load, the crack continues to grow stably until the instability condition of $K = K_{IC}$ and $dK/da = 0$, where the indent crack pops-in to form a straight-through precr ack with a size of a_{th}. If further subjected to increasing applied stress, the precrack grows stably, because $K \geq K_{IC}$, to a crack size of $a = a_{th} + \Delta a_{th}$, where K decreases with crack size, resulting in a crack arrest condition of $K \leq K_{IC}$ and $dK/da < 0$. The four distinct steps of precracking are summarized in figure 8.

EXPERIMENTAL RESULTS AND DISCUSSION

Precracking

Figure 9 shows the results of crack size measurements as a function of applied compressive load F_a for the two types of indent flaws: as-indented, and indented and annealed. For the as-indented flaws, the indent crack normal to the applied stress grows stably until $F_p = 11.9$ kN, where the stably grown indent crack pops-in because of the instability condition and forms a straight-through crack with a size of $a_{th} = 2$ mm. With further increasing load, the straight-through crack proceeds to grow stably. On the other hand, the annealed indent crack does not exhibit any stable crack growth because the residual stress has been relieved; it remains intact until instability at $F_p = 13.6$ kN, where the intact indent crack pops-in to form a straight-through crack with a size of $a_{th} = 2.5$ mm. Note that both F_p and a_{th} are greater in the annealed indent flaw than in the as-indented flaw, indicative of the residual stress effect, as reflected in equation (1). This precracking sequence for the indent flaw is in good qualitative agreement with the results shown in figure 7.

Configuration of Precrack

To ensure a good precrack (symmetrical and straight), it is essential that the loaded surfaces of the specimen and the upper and lower fixtures are as parallel as possible. Likewise, the indentation placed in the specimen center should be aligned in the center of the fixture span. Typical examples of precrack configurations are shown in figure 10, where the front and side views of the acceptable and unacceptable precracks are presented. The acceptability of a precrack was based on the requirements specified by ASTM E-399 (ref. 4). It was found that a good precrack could also be achieved by placing multiple indent cracks across the thickness of the specimen. This is particularly useful for some ceramic materials, such as SiC and Al_2O_3, which have relatively high porosities that generally inhibit well-defined indent crack patterns because of chipping and crushing. The effects of the number of indents on normalized precrack size a_{th}/W and precracking load are shown in figure 11 for the SiC whisker-reinforced silicon nitride material. Note that a_{th}/W and F_p are almost independent of the number of indents (up to three) since the spacing between the adjacent indent cracks is large; whereas, for the higher number of indents (up to seven), the effects are rapidly amplified because of the decreasing crack spacings.

Precracking Load Versus Indentation Load

Figure 12 summarizes the experimental data on F_p as a function of P for all the tested materials ($S = W = 6$ mm). This figure shows that as the indentation load increases the corresponding precracking load decreases.

The solid lines (which are based on eq. (8)) in the figures represent the best-fit lines with a slope of the $-1/3$ in the log F_p versus the log P plot. All the correlation coefficients of this functional fit analysis were higher than 0.920 except those for the silicon carbide material, indicating that the data fit to the theoretical equation (eq. (8)) is reasonably good. However, the silicon carbide material exhibited a lower correlation coefficient of 0.820, suggesting that the silicon carbide material does not follow the theoretical curve well because chipping and crushing produce an ill-defined indentation crack pattern in the specimen surface. Note that the higher indent loads produced more ill-defined indent cracks, thereby resulting in the poor correlation between F_p and P.

A typical result of α evaluated by strain gaging is presented in figure 13, where the maximum tensile stress (or strain) occurring in the specimen surface was plotted against applied compressive load F_a. This figure shows clearly that linear elasticity holds between $F_a - \sigma_{max}$. Linear regression analysis of these values gives $\alpha = 13.2 \pm 0.1$ MPa/kN. This result is for $S = W = 6$ mm in GN-10 SiC$_w$/silicon nitride.

Results of indentation strength versus indentation load for each test material are summarized in figure 14. Similar to the F_p-P relation (fig. 12), indentation strengths decrease with increasing indentation load. The solid lines (which are based on eq. (3)) in the figures represent the functional-fit lines with a slope of $-1/3$ in the log σ_f versus log P plot. The correlation coefficients were ≥ 0.930 for all the tested materials except the silicon carbide material. The silicon carbide material exhibited a poor correlation with a coefficient of 0.830, as in the F_p-P relation. With the use of the σ_f-P data in conjunction with the F_p-P data (fig. 12), the constant α was estimated on the basis of equations (3) and (6), and is presented in table II for all the test materials. Regardless of the test material, α is almost constant, with an average value of $\alpha = 13.3 \pm 0.9$ MPa/kN. The reason for α's insensitivity to the test materials is that the major material property, E (probably ν, too), does not differ significantly among the test materials, as seen in table I.

Figure 15 summarizes the constant α evaluated by strain gaging, finite element analysis, and the indentation strength method for different S and W. Here, $L = 18$ mm and $t = 3$ mm. It can be seen that the finite element solution agrees somewhat with experimentally evaluated data. Therefore, it can be concluded that equation (8) together with the α values in figure 15 can provide a relationship between F_p and P.

Precrack Size Versus Indentation Load

A summary of the experimental results of precrack size a_{th} versus indentation load P is shown in figure 16 with a_{th} normalized with respect to W. The figures show that a_{th} decreases with increasing P, and that for a given P, a_{th} increases with decreasing W and increasing S. A poor correlation between a_{th} and P was observed for the silicon carbide material because of the uncertainty in crack size measurements. For a given S and W, a_{th} is a weak function of P. The solid lines represent the best-fit lines to experimental data. Figure 17 illustrates a typical example of how to estimate a precrack size for a given indentation load (and K_{Ic}). The prediction here is made such that F_p is determined first from equation (8) with α for a given P, and then with this determined F_p, the corresponding a_{th} is obtained from data as shown in figure 6. Unfortunately, no closed-form solution is available for the a_{th}-P relation. An additional effort is in progress to include various combinations of S and W. It should be mentioned, however, that the experimental data shown in figures 12 and 16 can also be utilized as an engineering data base in SEPB precracking parameters.

Fracture Toughness Evaluation

Figure 18 summarizes the results of fracture toughness measurements as a function of normalized crack size a_{th}/W determined by the SEPB method for the five test materials. The fact that the fracture toughness is almost independent of crack size suggests that the tested materials do not exhibit any significant R-curve

7

behavior. However, moderate R-curve behavior has been observed in the alumina material by indentation strength and chevron-notch methods (ref. 8). Because of ill-defined crack front configurations, the K_{IC} determined for the silicon carbide material was considered inaccurate. Note that the K_{IC} for typical silicon carbide materials ranges between 2 and 3 MPa√m; therefore, the evaluated K_{IC} for NC 433 also appears unrealistically high ($\approx$ 5 MPa√m), as seen in figure 18. In fact, any indentation-induced K_{IC} measurements in silicon carbide materials have a similar limitation because a well-defined crack pattern is not formed. The chevron-notched beam method is strongly recommended for this type of material.

The K_{IC} values obtained by the SEPB method are tabulated in table III, where the K_{IC} values evaluated by the indentation strength (ref. 9) and the chevron-notched beam (ref. 10) methods (refs. 11 and 12) are also included for comparison. Although the K_{IC} values estimated by the SEPB method are slightly lower than those obtained by the indentation strength and chevron-notched beam methods, the overall agreement of the SEPB results with other results is excellent (except for the silicon carbide material), suggesting that the SEPB method is a convenient and simple means for evaluating the fracture toughness of ceramic materials. The SEPB method also has been successfully applied to mode I and II fracture behavior of Si_3N_4 (ref. 13). However, one important limitation in the SEPB method is that, at high temperatures, crack healing occurs readily in an air environment because of the combined effect of oxidation and the very small crack opening displacement present in the precrack (refs. 12 and 14). The use of an inert environment or the chevron-notched beam method is recommended for high-temperature (>1000 °C) K_{IC} evaluation.

SUMMARY OF RESULTS

The precracking parameters for ceramic single-edge-precracked-beam (SEPB) specimens were analyzed with the finite element analysis and the indentation strength methods.

1. A relationship between precracking load and indentation load was derived as a function of specimen and fixture configurations, and material constants (Young's modulus, material hardness, and fracture toughness). An excellent agreement was found between theory and experiment.

2. A prediction methodology relating the precrack size to the indentation load was presented on the basis of the relation between precracking and indentation loads and the numerically obtained precracking load versus precrack size relation.

3. A reasonable agreement in fracture toughness estimation was found between the SEPB and the indentation strength and chevron-notched beam methods for silicon nitride, alumina, and two silicon carbide whisker-reinforced silicon nitrides. However, an accurate fracture toughness value was not achieved for NC 433 silicon carbide because ill-defined crack patterns produced by indentation caused crooked precracks to form.

APPENDIX—SYMBOLS

a crack size

a_f critical crack size at instability, size at end of stable crack growth

a_i as-indented initial crack size

a_{th} size of straight-through precrack

8

E Young's modulus of specimen

F_a applied compressive load

F_p precracking load

H material hardness

K net stress intensity factor

K_a mode I applied stress intensity factor due to applied remote stress σ_a

K_{IC} specimen fracture toughness

K_r mode I stress intensity factor due to residual stresses produced by elastic/plastic mismatches of indentation

L contact length between upper silicon nitride plate and specimen

P indentation load

S inner span of fixture

t specimen thickness

W specimen width

α proportionality constant relating force applied to precracking fixture and maximum tensile stress induced in the specimen

Δa_i stable crack growth

ε_{max} maximum bending strain

ν Poisson ratio of specimen

Σ_r material/indenter geometry constant associated with residual contact stress

σ stress

σ_a applied remote stress

σ_f fracture strength

σ_{max} maximum bending stress

σ_{xx} normal stress parallel to the x axis

σ_{xy} shear stress in the xy plane

σ_{yy} normal stress parallel to the y axis

ϕ calibration constant (0.016 for Vickers indenter)

Ω crack geometry factor

ACKNOWLEDGMENTS

REFERENCES

1. Nose, T.; and Fujii, T.: Evaluation of Fracture Toughness for Ceramic Materials by a Single-Edge-Precracked-Beam Method. J. Am. Ceram. Soc., vol. 71, no. 5, 1988, pp. 328-333.

2. Warren, R.; and Johanneson, B.: Creation of Stable Cracks in Hard Metals Using "Bridge" Indentation. Powder Metall., vol. 27, no. 1, 1984, pp. 25-29.

3. Bar-On, I., et al.: Fracture Toughness of Ceramic Precracked Bend Bars. J. Am. Ceram. Soc., vol. 73, no. 8, 1990, pp. 2519-2522.

4. American Society for Testing and Materials. Standard Test Method for Plane-Strain Fracture Toughness of Metallic Materials. ASTM Standard E-399, 1983.

5. Murakami, Y., ed.: Stress Intensity Factors Handbook. Vol. 1, Pergamon Press, New York, 1987, pp. 16-17.

6. Marshall, D.B.; Lawn, B.R.; and Chantikul, P.: Residual Stress Effect in Sharp Contact Cracking: Part 2. J. Mater. Sci., vol. 14, 1979, pp. 2225-2235.

7. Anstis, G.R., et al.: A Critical Evaluation of Indentation Techniques for Measuring Fracture Toughness: I. J. Am. Ceram. Soc., vol. 64, no. 9, 1981, pp. 533-538.

8. Salem, J.A., et al.: Effects of Precracking Method on Fracture Properties of Alumina. Proceedings of Society of Experimental Mechanics Conference on Experimental Mechanics, Milwaukee, WI, June 10-13, 1991, Society of Experimental Mechanics, Bethel, CT, 1991, pp. 762-769.

9. Chantikul, P., et al.: A Critical Evaluation of Indentation Techniques for Measuring Fracture Toughness: II. J. Am. Ceram. Soc., vol. 64, no. 9, 1981, pp. 539-543.

10. Munz, D., et al.: Fracture Toughness Determination of Al_2O_3 Using Four-Point-Bend Specimens with Straight-Through and Chevron Notches. J. Am. Ceram. Soc., vol. 63, 1980, pp. 300-305.

11. Choi, S.R.; and Salem, J.A.: Strength, Toughness, and R-Curve Behaviors of SiC Whisker-Reinforced Composite Si_3N_4 With Reference to Monolithic Si_3N_4. To be published in J. Mater. Sci., 1992.

12. Choi, S.R.; and Salem, J.A.: Strength and Fracture Toughness of Monolithic and SiC Whisker-Reinforced Silicon Nitrides. Advanced Composite Materials, Ceramic Transactions, Vol. 19, American Ceramic Society, Westerville, OH, 1991, pp. 741-748.

13. Tikare, V.; and Choi, S.R.: The Influence of Microstructure on Combined Mode I and Mode II Toughness in Si_3N_4. Ceramic Engineering and Science Proceedings, 13th Annual Conference on Composites and Advanced Ceramic Materials, Part 1 of 2. Vol. 12, no., 7-8, Jul.-Aug. 1991, pp. 1437-1447.

14. Choi, S.R.; and Tikare, V.: Crack Healing in Silicon Nitride Due to Oxidation. Ceram. Eng. Sci. Proc., vol. 12, no. 9-10, 1991, pp. 2190-2202.

TABLE I.—PHYSICAL PROPERTIES OF TEST MATERIALS

Material	Young modulus,[a] E, GPa	Hardness,[b] H, GPa
Norton Si_3N_4	295	16.7
Norton SiC_w/Si_3N_4	305	19.4
Garrett SiC_w/Si_3N_4	330	16.0
96 percent Al_2O_3	324	10.0
NC 433 SiC	311	23.5

[a]Measured by strain gage.
[b]Measured by Vickers microhardness tester.

TABLE II.—EVALUATION OF PROPORTIONALITY CONSTANT, α, FROM INDENTATION DATA

[Span = width = 6 mm.]

Material	$F_pP^{1/3}$, kN-$N^{1/3}$	$\sigma_fP^{1/3}$, MPa-$N^{1/3}$	α,[a] MPa/kN
Norton Si_3N_4	65.7	787.7	12.01
Norton SiC_w/Si_3N_4	73.7	989.7	13.43
Garrett SiC_w/Si_3N_4	89.2	1277.3	14.32
96 percent Al_2O_3	46.4	632.3	13.62
NC 433 SiC	58.5	764.4	13.07
Average α = 13.3±0.9			

[a]$\alpha = \sigma_fP^{1/3}/F_pP^{1/3}$.

12

TABLE III.—SUMMARY OF FRACTURE TOUGHNESS, K_{IC}, ESTIMATIONS

Material	SEPB		Indent strength (refs. 11 and 12)		Chevron notch (refs. 10 to 12)	
	K_{IC}, MPa$\sqrt{m}$					
Norton Si_3N_4	3.50	[a]0.25	3.90	[a]0.05	4.30	[a]0.30
Norton SiC_w/Si_3N_4	4.62	.42	4.64	.03	4.90	.20
Garrett SiC_w/Si_3N_4	5.18	.41	5.53	.11	5.46	.28
96 percent Al_2O_3	3.09	.17	3.20	.21	3.67	.05

[a]Numbers in these columns represent one standard deviation.
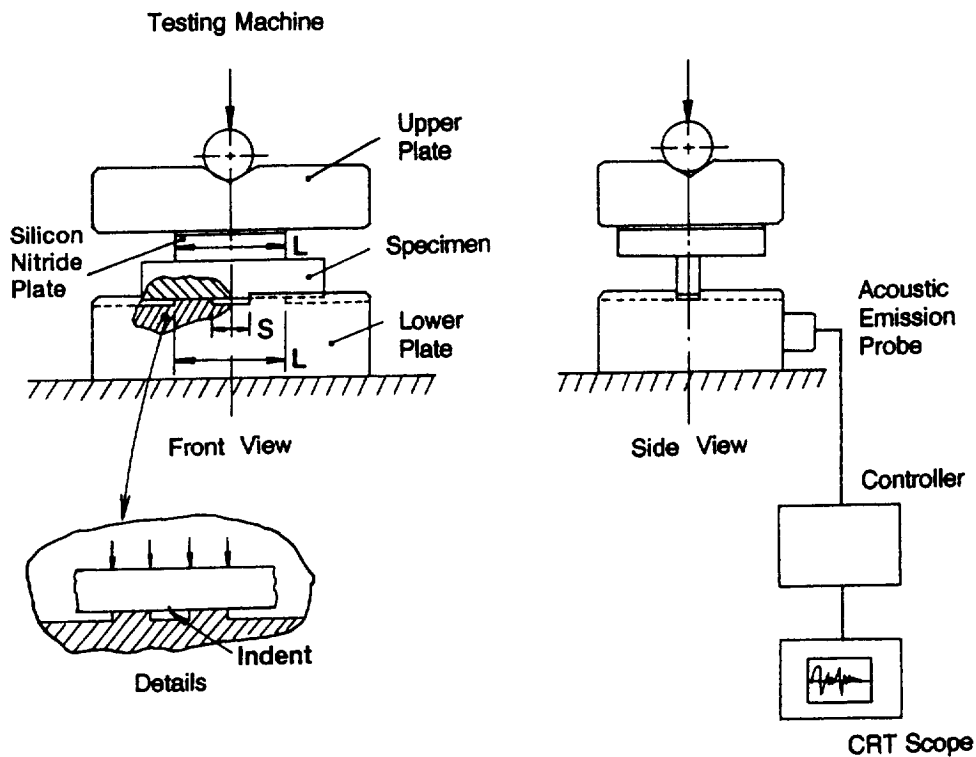
Figure 1.—Schematic of SEPB experimental apparatus. Span, S, 3 to 6 mm; length, L, 18 mm.
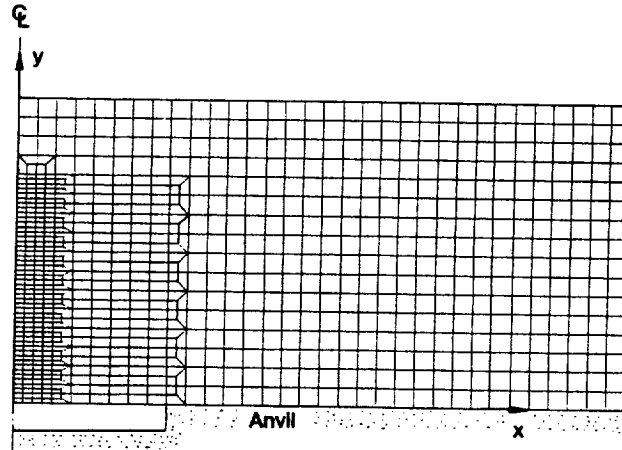
Figure 2.—Finite element mesh (half-plane). Compressive load is applied from the top surface of a specimen.

203.	A
166.	B
129.	C
92.4	D
55.7	E
18.9	F
-17.8	G
-54.5	H
-91.3	I
-128.	J
-165.	K
-201.	L
-238.	M
-275.	N
-312.	O
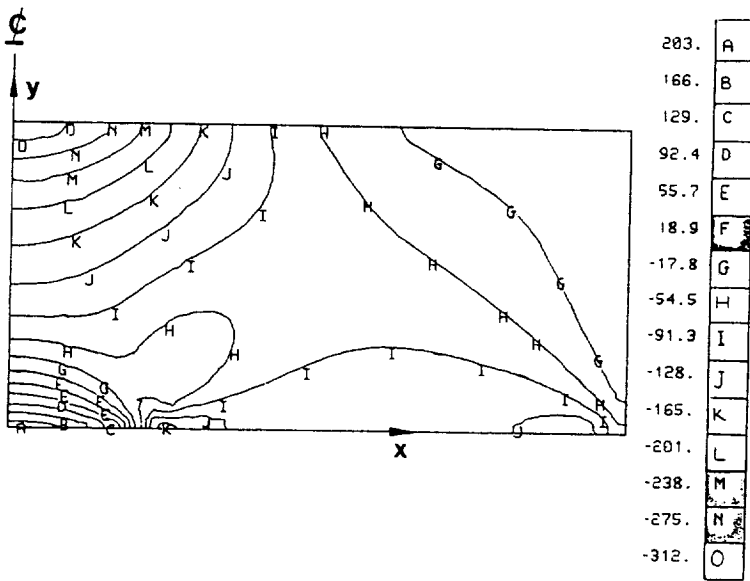
Figure 3.—Contours of σ_{xx} component (stress in MPa).
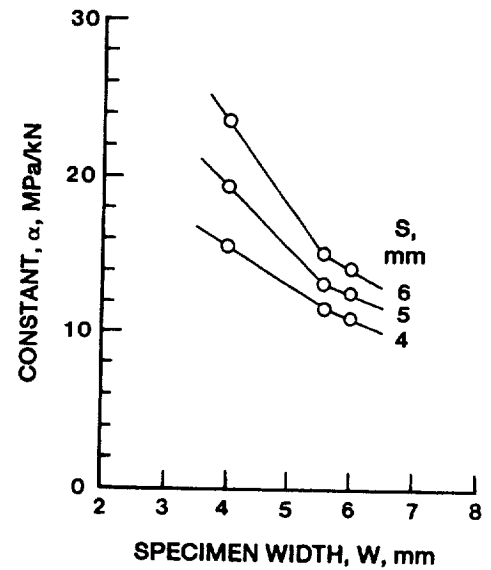
Figure 4.—Finite element analysis results of α as a function of specimen width, W, for different spans, S.

14
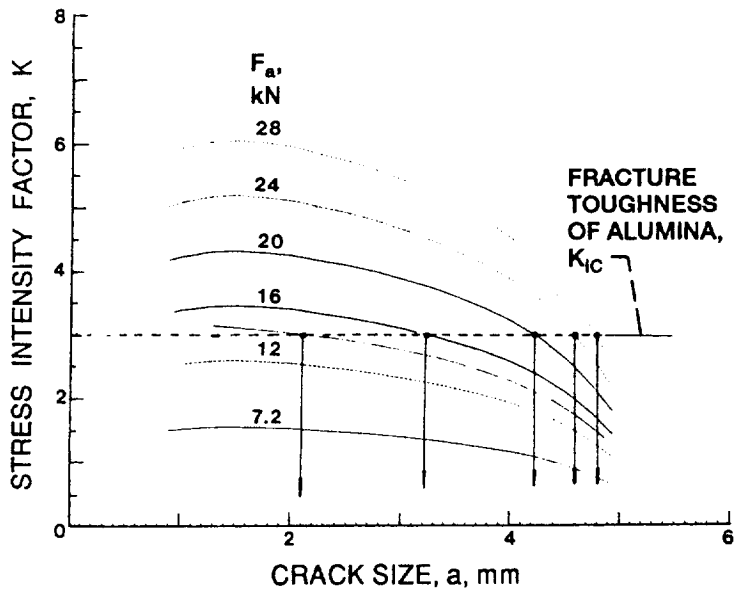
Figure 5.—Finite element analysis results of stress intensity factor as a function of precrack size for the straight-through crack and different precracking loads. Specimen span, S, and width, W, 6 mm.
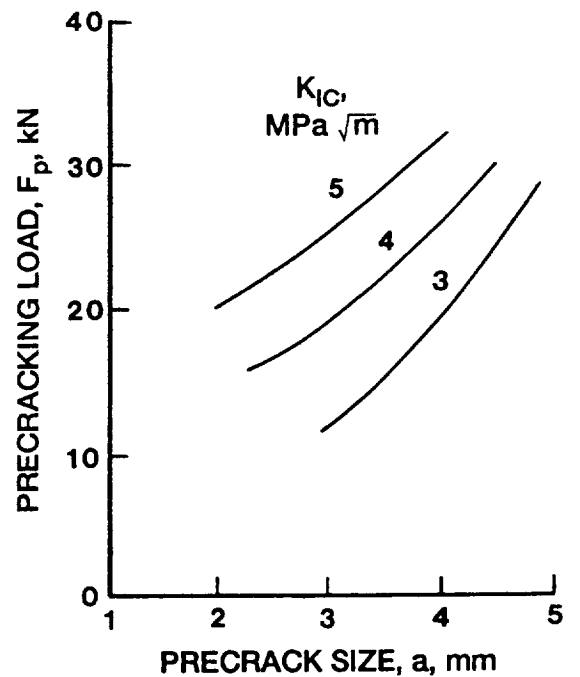
Figure 6.—Precracking load versus precrack size for different fracture toughnesses, K_{IC}'s, reconstructed from figure 5. Specimen span, S, and width, W, 6 mm.
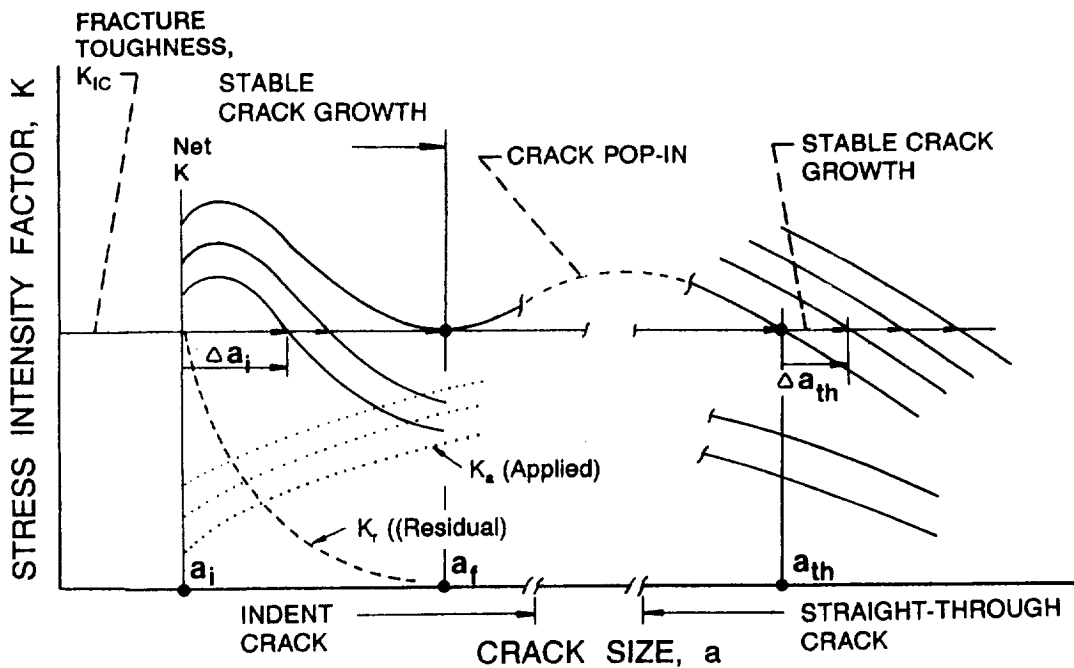
Figure 7.—Net stress intensity factor as a function of crack size with different levels of applied stress.

15

AS-INDENTED   STABLE CRACK GROWTH
OF INDENT CRACK

STABLE CRACK GROWTH OF   CRACK POP-IN TO FORM A
A STRAIGHT-THROUGH CRACK   STRAIGHT-THROUGH CRACK
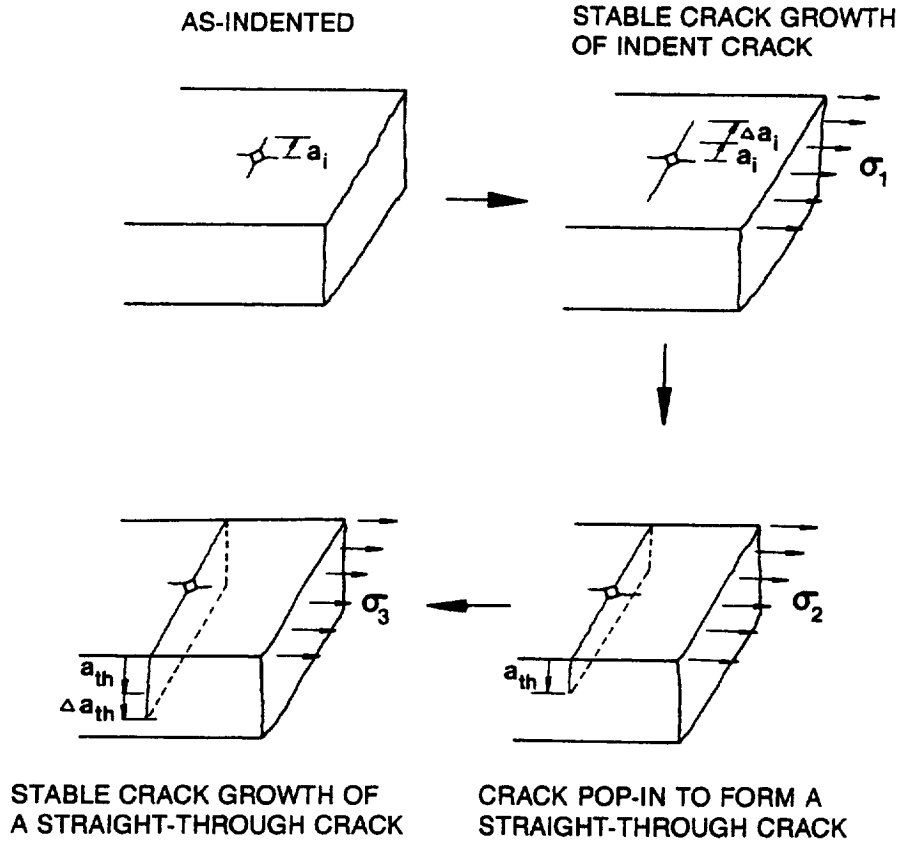
Figure 8.—Sequence of precracking from an indent flaw.
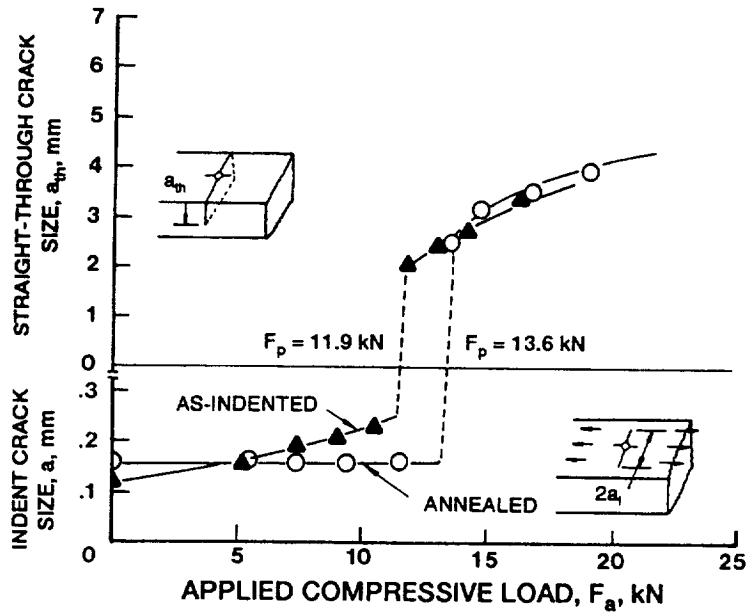
Figure 9.—Experimental results of crack size measurements as a function
of applied compressive load for two different types of indent flaws.
Material, Norton silicon nitride; span, S, and width, W, 6 mm; load, P,
98 N.

Acceptable
(Symmetric)
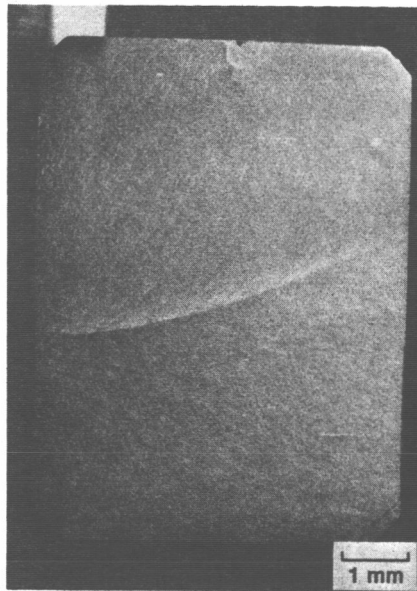
Unacceptable
(Not symmetric)

(a) Front view.
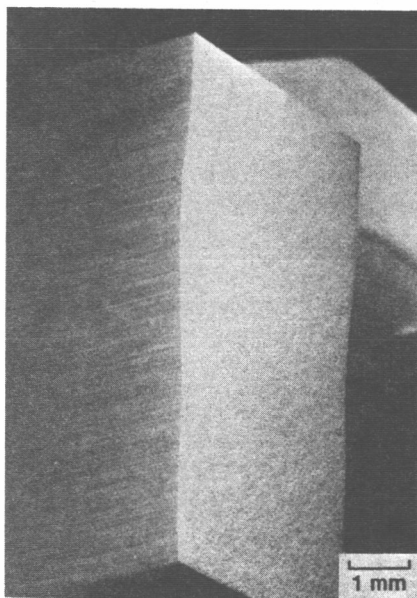
Acceptable
(Coplanar)
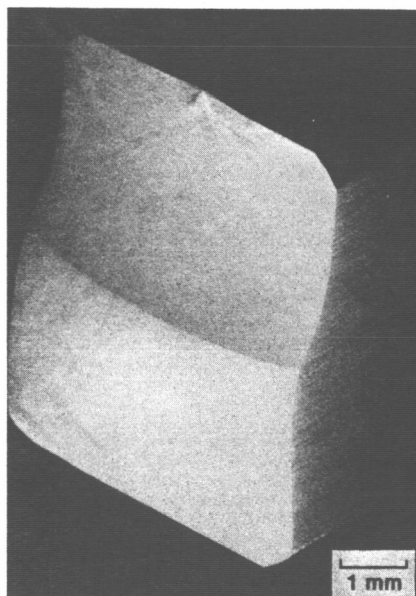
Unacceptable
(Not Coplanar)

(b) Side view.

Figure 10.—Configurations of precracks in fracture surfaces.
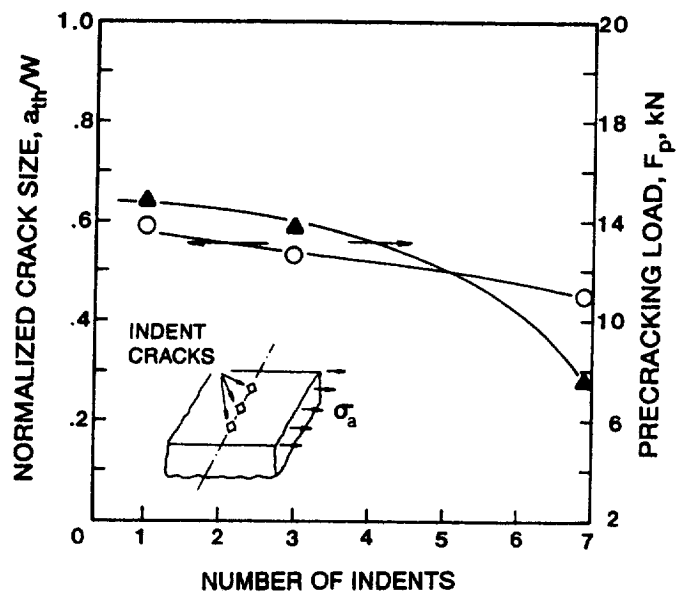
Figure 11.—Effects of number of indents on precracking load and precrack size. Material, GN-10 SIC$_w$/silicon nitride, span, S, 6 mm; width, W, 4 mm; load, P, 98 N.
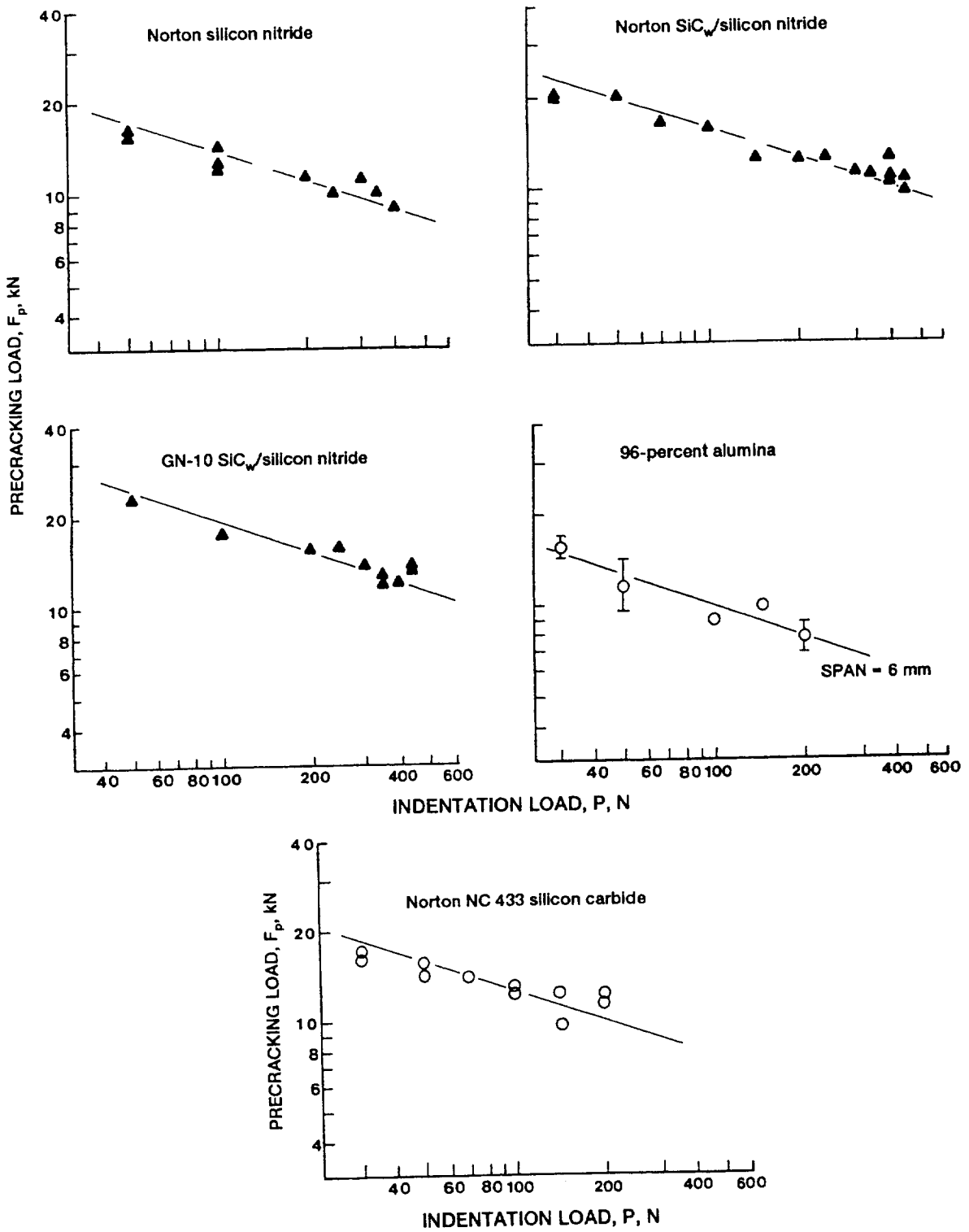
Figure 12.—Summary of experimental results on precracking load versus indentation load for five test materials. Span, S, and width, W, 6 mm.

19
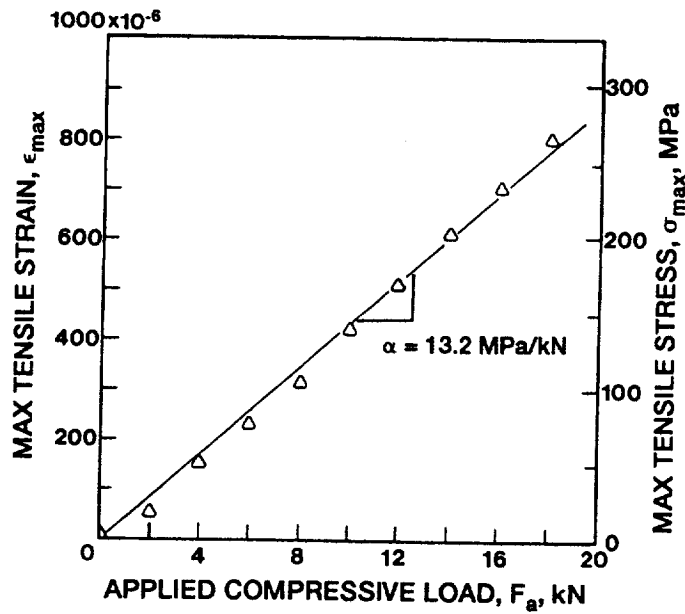
Figure 13.—Maximum applied stress as a function of applied compressive load obtained with strain gage. α represents a slope of σ_{max} versus F_a curve. Material, GN-10 SiC_w/silicon nitride; span, S, and width, W, 6 mm.
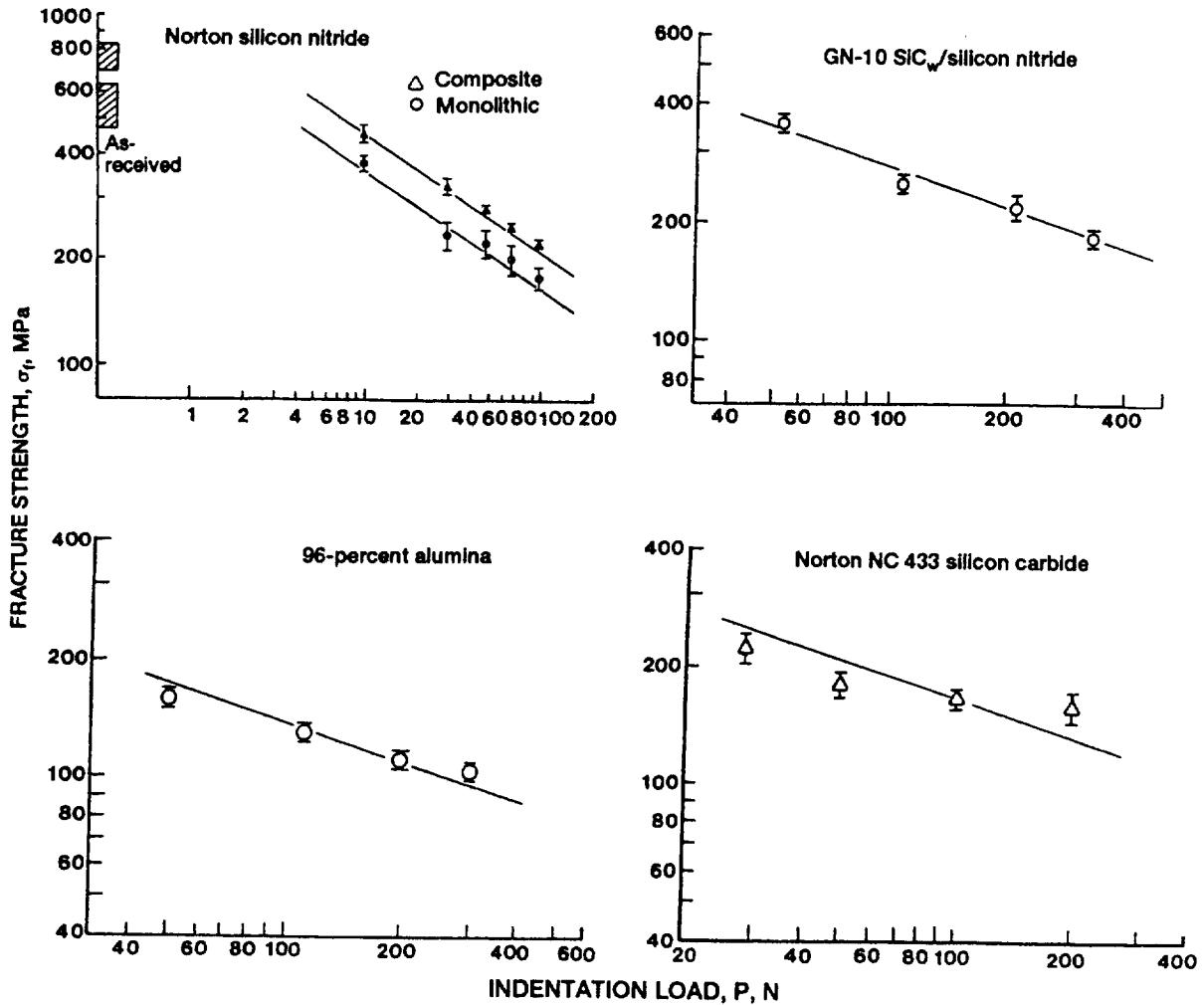
Figure 14.—Summary of experimental results on indentation strength as a function of indent load for five test materials.
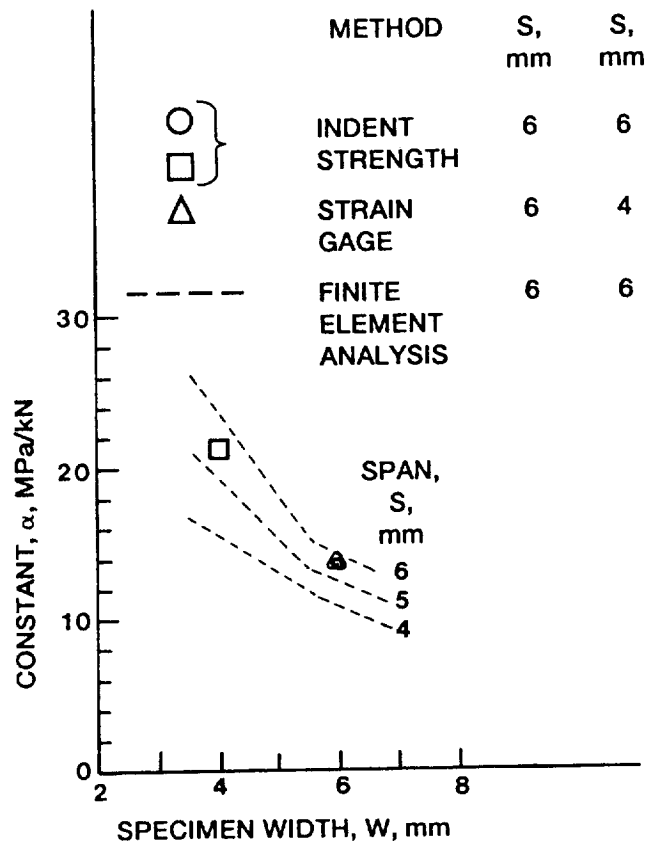
Figure 15.—Summary of α evaluated by finite element analysis, indentation strength, and strain gaging.
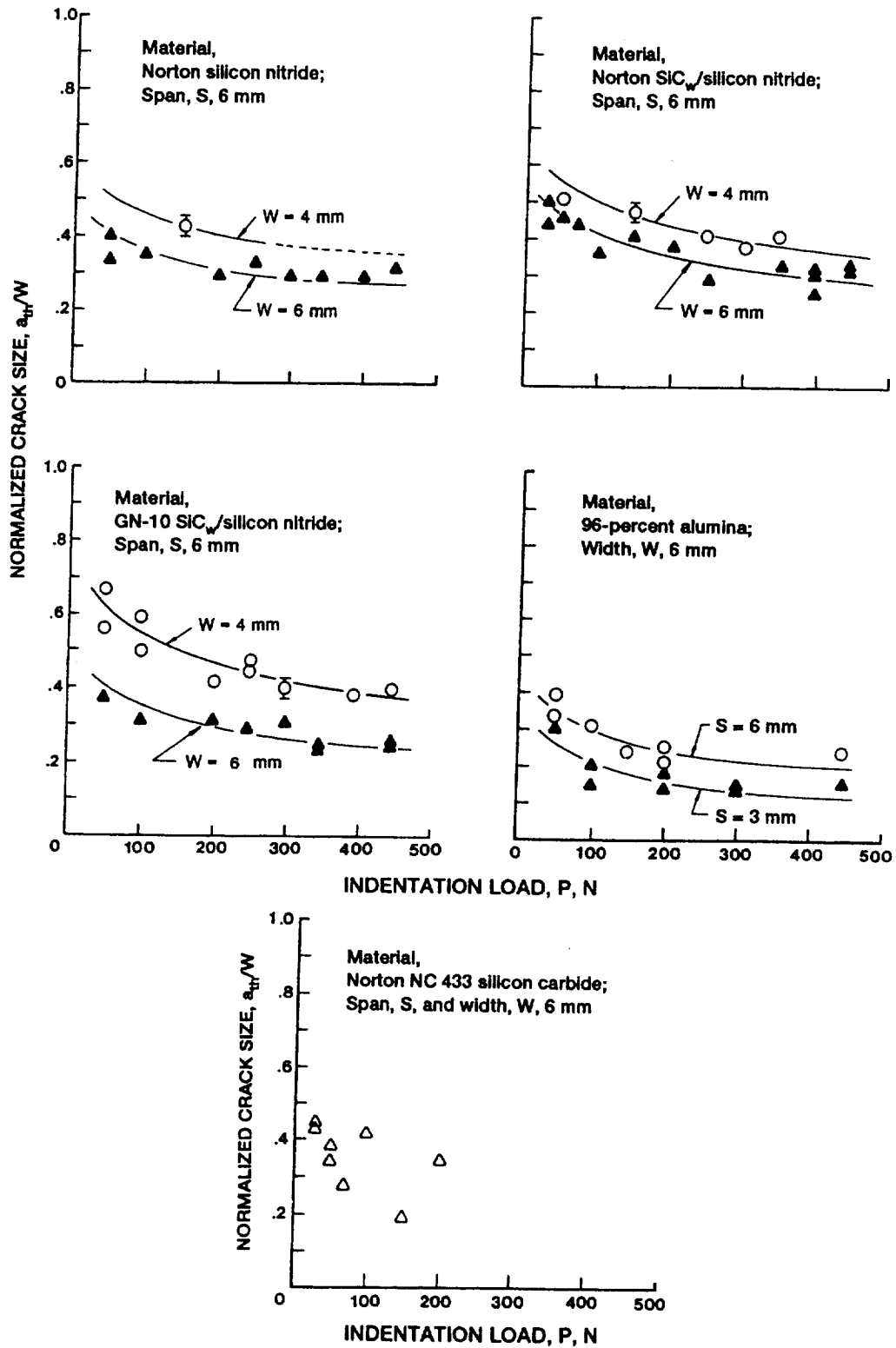
Figure 16.—Summary of experimental results on precracking size versus indentation load for five test materials.

EXPERIMENTAL PROCEDURES

The materials used in this study were silicon nitride with an equiaxed microstructure (Norton[1]), 96 percent alumina,[2] siliconized silicon carbide (Norton[3]), and two SiC whisker-reinforced (30 vol %) silicon nitrides (Norton[1] and Garrett[4]). The physical properties of the test materials are summarized in table I. All the specimens were in the form of flexure bars with 4- to 6-mm width, 3-mm thickness, and 25- to 50-mm length. The specimens were finished with a 320-grit diamond wheel, and the prospective tensile surface of each specimen was hand-polished with 600-grit SiC paper prior to indentation.

A Vickers microhardness indenter was used to make indents in the center of the polished surface of each specimen with the indentation diagonals parallel and perpendicular to the prospective tensile stress direction. Then the indented specimen was placed in the SEPB fixture such that the indent site was located exactly in the center of the lower fixture span (fig. 1). The specimen was loaded gradually by an Instron[5] servohydraulic testing machine (Model 8501) with a crosshead speed of 120 μm/min. Precracking was detected by an acoustic emission probe attached to the lower fixture in conjunction with a CRT display (fig. 1). The corresponding precracking load was monitored with the testing machine console. A wide range of indentation loads P from 30 to 440 N were used with experimental variables of span S from 3 to 6 mm and specimen width W from 4 to 6 mm. The outer span, as well as the contact length between the upper silicon nitride plate and the specimen L, was fixed to be 18 mm. The lengths of test specimens were typically 25 mm; however, it was found that specimen lengths between 18 and 50 mm did not have a significant effect on precracking load and precrack size.

The precracked specimens were fractured with a four-point bend fixture to determine their precrack sizes as well as fracture toughness K_{IC}. The precrack size of each fractured specimen was measured by a low-power optical microscope. A dye penetrant was used to demarcate the precrack front. An average precrack size was obtained by measuring the crack length at the center and at two positions midway between the center and the side surface of the specimen, as specified in ASTM E-399 (ref. 4). Fracture toughness was evaluated with the formulation developed by Nisitani and Mori (ref. 5).

Additional testing was carried out to measure crack size as a function of applied compressive load during loading. Two types of indent flaws were utilized: as-indented, and those annealed in 1250 °C N_2 gas to remove residual stress produced by indentation. The crack sizes were measured with an optical microscope during periodic interruptions of the tests. The chosen test material was Norton silicon nitride. One indentation load of $P = 98$ N was utilized.

The indentation strength data for each test material were determined for an indentation load range of $P = 50$ to 300 N to provide additional information regarding the stress distribution developed in the specimen during precracking. Three specimens were used at each indent load. This was considered sufficient for the very low standard deviation of the indent strength (<5 percent).

---

[1]Norton Co., Northboro, MA. No commercial designation; this material was custom made for NASA.

[2]ALSIMAG 614 96 wt % alumina; G.E. Ceramics, Laurens, SC.

[3]NC 433; Norton Co., Northboro, MA.

[4]GN 10 + 30% SiC_w; Garrett Ceramic Components, Allied Signal, Torrance, CA.

[5]Instron, Canton, MA.

REPORT DOCUMENTATION PAGE

1. AGENCY USE ONLY (Leave blank)	2. REPORT DATE	3. REPORT TYPE AND DATES COVERED
	August 1992	Technical Memorandum

4. TITLE AND SUBTITLE

Analysis of Precracking Parameters and Fracture Toughness for Ceramic Single-Edge-Precracked-Beam Specimens

5. FUNDING NUMBERS

WU-505-63-M

6. AUTHOR(S)

Sung R. Choi, Abhisak Chulya, and Jonathan A. Salem

7. PERFORMING ORGANIZATION NAME(S) AND ADDRESS(ES)

National Aeronautics and Space Administration
Lewis Research Center
Cleveland, Ohio 44135-3191

8. PERFORMING ORGANIZATION REPORT NUMBER

E-6893

9. SPONSORING/MONITORING AGENCY NAMES(S) AND ADDRESS(ES)

National Aeronautics and Space Administration
Washington, D.C. 20546-0001

10. SPONSORING/MONITORING AGENCY REPORT NUMBER

NASA TM-105568

12a. DISTRIBUTION/AVAILABILITY STATEMENT

Unclassified - Unlimited
Subject Category 27

12b. DISTRIBUTION CODE

13. ABSTRACT (Maximum 200 words)

The single-edge-precracked-beam (SEPB) method involves creation of a straight-through crack from an indentation crack. The straight-through crack is developed by applying a controlled bending load to a specimen via a precracking fixture. The fixture induces a sequence of (1) stable growth of the indentation crack, (2) pop-in, and then (3) arrest — thereby forming a straight-through precrack. The effects of indentation load on precracking load as well as precrack size were studied for experimental variables such as specimen width, fixture span, and material. Finite element analysis was used to obtain the stress distribution and stress intensity factor, thus providing a quantitative prediction of the precracking load and precrack size for silicon nitride, alumina, silicon carbide, and two SiC whisker-reinforced silicon nitrides. Fracture toughness values obtained from the SEPB method were compared with those obtained from other methods.

14. SUBJECT TERMS

Fracture toughness; Ceramics; Single-edge-precracked-beam (SEPB) method; Precracking

15. NUMBER OF PAGES

24

16. PRICE CODE

A03

17. SECURITY CLASSIFICATION OF REPORT	18. SECURITY CLASSIFICATION OF THIS PAGE	19. SECURITY CLASSIFICATION OF ABSTRACT	20. LIMITATION OF ABSTRACT
Unclassified	Unclassified	Unclassified	